An Interactive Shader for Natural Diffraction Gratings

Bachelorarbeit

der Philosophisch-naturwissenschaftlichen Fakultät
der Universität Bern

vorgelegt von

Michael Single

2014

Leiter der Arbeit:
Prof. Dr. Matthias Zwicker
Institut für Informatik und angewandte Mathematik

Abstract

Inhaltsverzeichnis

Kapitel 1

Derivations

1.1 Problem Statement and Challenges

The goal of this thesis is to perform a physically accurate and interactive simulation of structural colors production like shown in figure 1.2, which we can see whenever a light source is diffracted on a natural grating. For this purpose we need the to be provided by the following input data as shown in figure 1.1:

- A mesh representing a snake surface[1] with associated texture coordinates as shown in figure 1.1(a).
- A natural diffraction grating represented as a height field, its maximum height and its pixel-width-correspondence[2].
- A vectorfield which describes how fingers on a provided surface of the nanostructrue are aligned as shown in figure 1.1(c).

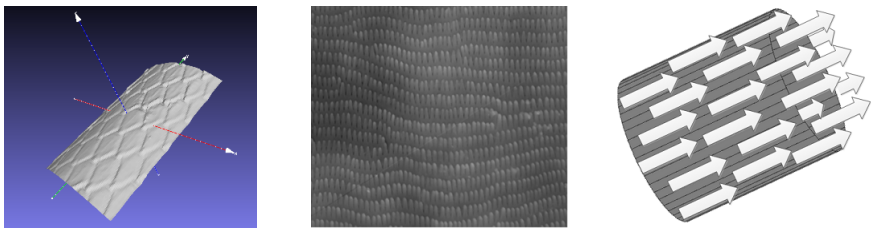

(a) Structure Geometry (b) Nanostructure Surface (c) Patch Orientation

Abbildung 1.1: Input for our simulation

We want to rely on the integral equation **??** derived by J. Stam in his paper [Sta99] about diffraction shaders. This equation formualtes a BRDF modeling

[1] Which is in our simulation an actual reconstruction of a real snake skin. These measurements are provided by the Laboratory of Artificial and Natural Evolition at Geneva.See their website:`www.lanevol.org`.

[2] Since the nanostructure is stored as a grayscale image, we need a scale telling us what length and height one pixel cooresponds to in this provided image.

the effect of diffraction under the assumption that a given grating can either be formulated as an analytical function or its structure is simple enough beeing modeled relying on statistical methods. These assumptions guarantee that **??** has an explicit solution. However, the complexisty of a biological nanostructures cannot sufficiently and accurately modeled simply using statistical methods. This is why interactive computation at high resolution becomes a hard task, since we cannot evaluate the given integral equation on the fly. Therefore, we have to adapt Stam's equation such that we are able to perform interactive rendering using explicitly provided height fields.

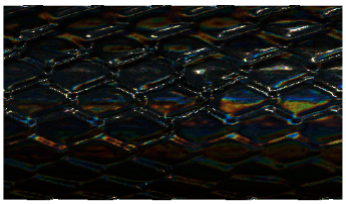

Abbildung 1.2: Output: Rendered Structural Colors

1.2 Rendering Equation

As already seen in the theoretical background chapter, colors are associated to radiance. Since we are starting with Stam's BRDF[3] formulation but want to perform a simulation rendering structural colors, we have to reformulate this BRDF equation such that we will end up with an identity of the reflected spectral radiance. This is where the rendering equation comes into play. Lets assume we have given an incoming light source with solid angle ω_i and θ_i is its angle of incidence, ω_r is the solid angle for the reflected light. Further let λ denote the wavelength and Ω is the hemisphere we of integration for the incoming light. Then, we are able to formulate a BRDF by using its definition **??**:

$$\begin{aligned}
f_r(\omega_i,\omega_r) &= \frac{dL_r(\omega_r)}{L_i(\omega_i)cos(\theta_i)d\omega_i} \\
\Rightarrow f_r(\omega_i,\omega_r)L_i(\omega_i)cos(\theta_i)d\omega_i &= dL_r(\omega_r) \\
\Rightarrow \int_\Omega f_r(\omega_i,\omega_r)L_i(\omega_i)cos(\theta_i)d\omega_i &= \int_\Omega dL_r(\omega_r) \\
\Rightarrow L_r(\omega_r) &= \int_\Omega f_r(\omega_i,\omega_r)L_i(\omega_i)cos(\theta_i)d\omega_i \qquad (1.1)
\end{aligned}$$

The last equation is the so called rendering equation. We assume that our incident light is a directional, unpolarized light source **??** like sunlight and therefore its radiance is given as

$$L_\lambda(\omega) = I(\lambda)\delta(\omega - \omega_i) \qquad (1.2)$$

where $I(\lambda)$ is the intensity of the relative spectral power for the wavelength λ. Since all light rays are parallel, whenever we are provided by a directional

[3]Remember that a BRDF is the portion of a incident light source reflected off a given surface towards a specified viewing direction

light source and we can think of radiance as a measure of the light emitted from a particular surface location into a particular direction, above's radiance identity will follow immediately. By plugging the identity 1.2 into our current rendering equation 1.1, we will get:

$$\begin{aligned} L_\lambda(w_r) &= \int_\Omega BRDF_\lambda(\omega_i, \omega_r) L_\lambda(\omega_i) cos(\theta_i) d\omega_i \\ &= BRDF_\lambda(\omega_i, \omega_r) I(\lambda) cos(\theta_i) \end{aligned} \tag{1.3}$$

where $L_\lambda(\omega_i)$ is the incoming radiance and $L_\lambda(\omega_r)$ is the radiance reflected by the given surface. Note that the integral in equation 1.3 vanishes since $\delta(\omega - \omega_i)$ is only equal one if and only if $\omega = \omega_i$.

1.3 Adaption of Stam's BRDF discrete height fields

We are going to use Stam's main derivation (**??**) for the $BRDF(\omega_i, \omega_r)$ in 1.3 by applying the fact that the wavenumber is equal $k = \frac{2\pi}{\lambda}$:

$$\begin{aligned} BRDF(\omega_i, \omega_r) &= \frac{k^2 F^2 G}{4\pi^2 A w^2} \langle |P(ku, kv)|^2 \rangle \\ &= \frac{4\pi^2 F^2 G}{4\pi^2 A \lambda^2 w^2} \langle |P(ku, kv)|^2 \rangle \\ &= \frac{F^2 G}{A\lambda^2 w^2} \langle \left| P(\frac{2\pi u}{\lambda}, \frac{2\pi v}{\lambda}) \right|^2 \rangle \end{aligned} \tag{1.4}$$

Going back to equation 1.3 and plugging equation 1.4 into it, using the definition of equation **??** and the equation 1.8 for ω we will get the following:

$$\begin{aligned} L_\lambda(\omega_r) &= \frac{F^2(1 + \omega_i \cdot \omega_r)^2}{A\lambda^2 cos(\theta_i) cos(\theta_r) \omega^2} \left\langle \left| P\left(\frac{2\pi u}{\lambda}, \frac{2\pi v}{\lambda}\right) \right|^2 \right\rangle cos(\theta_i) I(\lambda) \\ &= I(\lambda) \frac{F^2(1 + \omega_i \cdot \omega_r)^2}{\lambda^2 A \omega^2 cos(\theta_r)} \left\langle \left| P\left(\frac{2\pi u}{\lambda}, \frac{2\pi v}{\lambda}\right) \right|^2 \right\rangle \end{aligned} \tag{1.5}$$

Note that the fresnel term F is actually a function of (w_i, w_r) but in order to keep it simple, we omitted its arguemts. So far we just plugged Stam's BRDF identity into the rendering equation and hence have not significantly deviated from his formulation. Keep in mind that P deontes the Fourier transform of the provided height field which depends on the viewing and light incidence direction. Thus this Fourier Transform has to be recomputed for every direction. One particular strategy to solve this issue is to approximate P by the Discrete Fourier Transform (DFT)[4] and seperate its computation such that terms for many directions can be precomputed and then later retrieved by look ups.

[4]See appendix A for further information

1.4 Reproduce FT by DTFT

$$
\begin{aligned}
L_\lambda(\omega_r) &= \frac{F(\omega_i,\omega_r)^2(1+\omega_i\cdot\omega_r)^2}{A\lambda^2 cos(\theta_i)cos(\theta_r)(cos(\theta_i)+cos(\theta_r))^2}\left\langle\left|P\left(\frac{2\pi u}{\lambda},\frac{2\pi v}{\lambda}\right)\right|^2\right\rangle cos(\theta_i)I(\lambda)\\
&= I(\lambda)\frac{F(\omega_i,\omega_r)^2(1+\omega_i\cdot\omega_r)^2}{\lambda^2 A(cos(\theta_i)+cos(\theta_r))^2 cos(\theta_r)}\left\langle\left|P\left(\frac{2\pi u}{\lambda},\frac{2\pi v}{\lambda}\right)\right|^2\right\rangle\\
&= I(\lambda)\frac{F(\omega_i,\omega_r)^2(1+\omega_i\cdot\omega_r)^2}{\lambda^2 A(cos(\theta_i)+cos(\theta_r))^2 cos(\theta_r)}\left\langle\left|T_0^2 P_{dtft}\left(\frac{2\pi u}{\lambda},\frac{2\pi v}{\lambda}\right)\right|^2\right\rangle
\end{aligned}
\tag{1.6}
$$

Furthermore T_0 the sampling distance for the discretization of $p(x,y)$ assuming equal and uniform sampling in both dimensions x and y.

1.5 Special Coherence and Windowing

1.6 Reproduce DTFT by DFT

1.7 Optimization using Taylor Series

1.8 Spectral Rendering

1.8.1 BRDF formulation

1.8.2 Relative Reflectance

In this section we are going to explain how to scale our BRDF formulation such that all of its possible output values are mapped into the range $[0,1]$. Such a relative reflectance formulation will ease our life for later rendering purposes since usually color values are within the range $[0,1]$, too. Furthermore, this will allow us to properly blend the resulting illumination caused by diffraction with a texture map.

Let us examine what $L_\lambda(\omega_r)$ will be for $\omega_r = \omega_0 := (0,0,*)$ i.e. specular reflection case, denoted as $L_\lambda^{spec}(\omega_0)$. When we know the expression for $L_\lambda^{spec}(\omega_0)$ we would be able to compute the relative reflected radiance for our problem 1.5 by simply taking the fraction between $L_\lambda(\omega_r)$ and $L_\lambda^{spec}(\omega_0)$ which is denoted by:

$$
\rho_\lambda(\omega_i,\omega_r) = \frac{L_\lambda(\omega_r)}{L_\lambda^{spec}(\omega_0)} \tag{1.7}
$$

Going back to the definition **??** of $(u,v,w) = -\omega_i - \omega_r$ and using spherical coordinates *B.2*, we get for w the following identity

$$
\begin{aligned}
w &= -\omega_i - \omega_r\\
&= -(\omega_i + \omega_r)\\
&= -\left(cos(\theta_i) + cos(\theta_r)\right)
\end{aligned}
\tag{1.8}
$$

and therefore w^2 is equal $(cos(\theta_i) + cos(\theta_r))^2$.
But first, let us derive the following expression:

$$\begin{aligned} L_\lambda^{spec}(\omega_0) &= I(\lambda)\frac{F(\omega_0,\omega_0)^2(1+\begin{pmatrix}0\\0\\1\end{pmatrix}\cdot\begin{pmatrix}0\\0\\1\end{pmatrix})^2}{\lambda^2 A(cos(0)+cos(0))^2 cos(0)}\langle\left|T_0^2 P_{dtft}(0,0)\right|^2\rangle \\ &= I(\lambda)\frac{F(\omega_0,\omega_0)^2(1+1)^2}{\lambda^2 A(1+1)^2 1}\left|T_0^2 N_{sample}\right|^2 \\ &= I(\lambda)\frac{F(\omega_0,\omega_0)^2}{\lambda^2 A}\left|T_0^2 N_{sample}\right|^2 \end{aligned} \tag{1.9}$$

Where $N_{samples}$ is the number of samples of the DTFT $A.3$. Thus, we can plug our last derived expression 1.9 into the definition for the relative reflectance radiance 1.7 in the direction w_r and will get:

$$\begin{aligned} \rho_\lambda(\omega_i,\omega_r) &= \frac{L_\lambda(\omega_r)}{L_\lambda^{spec}(\omega_0)} \\ &= \frac{I(\lambda)\frac{F(\omega_i,\omega_r)^2(1+\omega_i\cdot\omega_r)^2}{\lambda^2 A(cos(\theta_i)+cos(\theta_r))^2 cos(\theta_r)}\langle\left|T_0^2 P_{dtft}(\frac{2\pi u}{\lambda},\frac{2\pi v}{\lambda})\right|^2\rangle}{I(\lambda)\frac{F(\omega_0,\omega_0)^2}{\lambda^2 A}\left|T_0^2 N_{sample}\right|^2} \\ &= \frac{F^2(\omega_i,\omega_r)(1+\omega_i\cdot\omega_r)^2}{F^2(\omega_0,\omega_0)(cos(\theta_i)+cos(\theta_r))^2 cos(\theta_r)}\langle\left|\frac{P_{dtft}(\frac{2\pi u}{\lambda},\frac{2\pi v}{\lambda})}{N_{samples}}\right|^2\rangle \end{aligned} \tag{1.10}$$

For simplification and a better overview, let us introduce the following expression, the so called gain-factor:

$$C(\omega_i,\omega_r) = \frac{F^2(\omega_i,\omega_r)(1+\omega_i\cdot\omega_r)^2}{F^2(\omega_0,\omega_0)(cos(\theta_i)+cos(\theta_r))^2 cos(\theta_r) N_{samples}^2} \tag{1.11}$$

Using this substitute, we will end up with the following expression for the relative reflectance radiance from equation 1.10:

$$\rho_\lambda(\omega_i,\omega_r) = C(\omega_i,\omega_r)\langle\left|P_{dtft}(\frac{2\pi u}{\lambda},\frac{2\pi v}{\lambda})\right|^2\rangle \tag{1.12}$$

Using the previous definition for the relative reflectance radiance 1.7:

$$\rho_\lambda(\omega_i,\omega_r) = \frac{L_\lambda(\omega_r)}{L_\lambda^{spec}(\omega_0)} \tag{1.13}$$

Which we can rearrange to the expression:

$$L_\lambda(\omega_r) = \rho_\lambda(\omega_i,\omega_r) L_\lambda^{spec}(\omega_0) \tag{1.14}$$

Let us choose $L_\lambda^{spec}(w_0) = S(\lambda)$ such that is has the same profile as the relative spectral power distribution of CIE Standard Illuminant $D65$ discussed

in **??**. Furthermore, when integrating over λ for a specular surface, we should get CIE_{XYZ} values corresponding to the white point for $D65$. The corresponding tristimulus values using CIE colormatching functions **??** for the CIE_{XYZ} values look like:

$$\begin{aligned} X &= \int_\lambda L_\lambda(\omega_r)\overline{x}(\lambda)d\lambda \\ Y &= \int_\lambda L_\lambda(\omega_r)\overline{y}(\lambda)d\lambda \\ Z &= \int_\lambda L_\lambda(\omega_r)\overline{z}(\lambda)d\lambda \end{aligned} \tag{1.15}$$

where $\overline{x}$, $\overline{y}$, $\overline{z}$ are the color matching functions. Using our last finding 1.14 for $L_\lambda(\omega_r)$ with the definition for the tristimulus values 1.15, we can actually derive an expression for computing the colors for our initial BRDF formula 1.1. Without any loss of generality it satisfies to derive an explicit expression for just one tristimulus term, for example X. Since The other have a similar formulation, except the we have to replace all X with Y or Z respectively. Therefore, we get:

$$\begin{aligned} X &= \int_\lambda L_\lambda(\omega_r)\overline{x}(\lambda)d\lambda \\ &= \int_\lambda \rho_\lambda(\omega_i,\omega_r)L_\lambda^{spec}(\omega_0)\overline{x}(\lambda)d\lambda \\ &= \int_\lambda \rho_\lambda(\omega_i,\omega_r)S(\lambda)\overline{x}(\lambda)d\lambda \\ &= \int_\lambda C(\omega_i,\omega_r)\langle\left|P_{dtft}(\frac{2\pi u}{\lambda},\frac{2\pi v}{\lambda})\right|^2\rangle S(\lambda)\overline{x}(\lambda)d\lambda \\ &= C(\omega_i,\omega_r)\int_\lambda\langle\left|P_{dtft}(\frac{2\pi u}{\lambda},\frac{2\pi v}{\lambda})\right|^2\rangle S(\lambda)\overline{x}(\lambda)d\lambda \\ &= C(\omega_i,\omega_r)\int_\lambda\langle\left|P_{dtft}(\frac{2\pi u}{\lambda},\frac{2\pi v}{\lambda})\right|^2\rangle S_x(\lambda)d\lambda \end{aligned} \tag{1.16}$$

Where we used the definition $S_x(\lambda)\overline{x}(\lambda)$ in the last step.

1.8.3 Taylor approximation for BRDF

In this section, we will deliver an approximation for the inverse Fourier Transformation of Stam's auxiliary function $p(x,y)$. This derivation will rely on the definition of Taylor Series expansion $A.8$. Further, we will provide an error bound for our approximation approach for a given number of iterations. Last, we will extend our current BRDF formula by the findings derived within this section.

Given $p(x,y) = e^{ikw\hbar(x,y)}$ form Stam's Paper **??** where $h(x,y)$ is a given height field. Let be y real or even complex value, and lets consider the power series for the the exponential function

$$e^t = 1 + t + \frac{t^2}{2!} + \frac{t^3}{3!} + ... = \sum_{n=0}^{\infty}\frac{t^n}{n!} \tag{1.17}$$

Let us define

$$t = t(x,y) = ikwh(x,y) \tag{1.18}$$

where i is the imaginary number. For simplification, let us denote $h(x,y)$ as h. Then it follows by our previous stated identities:

$$\begin{aligned} e^t &= 1 + (ikwh) + \frac{1}{2!}(ikwh)^2 + \frac{1}{3!}(ikwh)^3 + ... \\ &= \sum_{n=0}^{\infty} \frac{(ikwh)^n}{n!}. \end{aligned} \tag{1.19}$$

Hence it holds $p(x,y) = \sum_{n=0}^{\infty} \frac{(ikwh(x,y))^n}{n!}$. Let us now compute the Fourier Transformation of p(x,y) form above:

$$\begin{aligned} \mathcal{F}\{p\}(u,v) &= \mathcal{F}\left\{ \sum_{n=0}^{\infty} \frac{(ikwh)^n}{n!}. \right\}(u,v) \\ &=^{\mathcal{F}\, lin\, Operator} \sum_{n=0}^{\infty} \mathcal{F}\left\{ \frac{(ikwh)^n}{n!} \right\}(u,v) \\ &= \sum_{n=0}^{\infty} \frac{(ikw)^n}{n!} \mathcal{F}\{h^n\}(u,v) \end{aligned} \tag{1.20}$$

Therefore it follows: $P(\alpha,\beta) = \sum_{n=0}^{\infty} \frac{(ikw)^n}{n!} \mathcal{F}\{h^n\}(\alpha,\beta)$ for which $\mathcal{F}_{FT}\{h^n\}(u,v)$. Next we are going to look for an $N \in \mathbb{N}$ such that

$$\sum_{n=0}^{N} \frac{(ikwh)^n}{n!} \mathcal{F}\{h^n\}(\alpha,\beta) \approx P(\alpha,\beta) \tag{1.21}$$

is a good approximation. But first the following two facts have to be proven:

1. Show that there exist such an $N \in \mathbb{N}$s.t the approximation holds true.
2. Find a value for B s.t. this approximation is below a certain error bound, for example machine precision ϵ.

Proof Sketch of 1.

By the **ratio test** (see [**1**]) It is possible to show that the series $\sum_{n=0}^{N} \frac{(ikwh)^n}{n!} \mathcal{F}\{h^n\}(\alpha,\beta)$ converges absolutely:

Proof: Consider $\sum_{k=0}^{\infty} \frac{y^n}{n!}$ where $a_k = \frac{y^k}{k!}$. By applying the definition of the ratio test for this series it follows:

$$\forall y : limsup_{k\to\infty} |\frac{a_{k+1}}{a_k}| = limsup_{k\to\infty} \frac{y}{k+1} = 0 \tag{1.22}$$

Thus this series converges absolutely, no matter what value we will pick for y.

Part 2: Find such an N
Let $f(x) = e^x$. We can formulate its Taylor-Series, stated above. Let $P_n(x)$denote the n-th Taylor polynom,

$$P_n(x) = \sum_{k=0}^{n} \frac{f^{(k)}(a)}{k!}(x-a)^k \tag{1.23}$$

where a is our developing point (here a is equal zero).

We can define the error of the n-th Taylor polynom to be $E_n(x) = f(x) - P_n(x)$. the error of the n-th Taylor polynom is difference between the value of the function and the Taylor polynomial This directly implies $|E_n(x)| = |f(x) - P_n(x)|$. By using the Lagrangian Error Bound it follows:

$$|E_n(x)| \leq \frac{M}{(n+1)!}|x-a|^{n+1} \tag{1.24}$$

with $a = 0$, where **M** is some value satisfying $|f^{(n+1)}(x)| \leq M$ on the interval $I = [a, x]$. Since we are interested in an upper bound of the error and since **a** is known, we can reformulate the interval as $I = [0, x_{max}]$, where

$$x_{max} = \|i\| k_{max} w_{max} h_{max} \tag{1.25}$$

We are interested in computing an error bound for $e^{ikwh(x,y)}$. Assuming the following parameters and facts used within Stam's Paper:

- Height of bump: 0.15micro meters
- Width of a bump: 0.5micro meters
- Length of a bump: 1micro meters
- $k = \frac{2\pi}{\lambda}$ is the wavenumber, $\lambda \in [\lambda_{min,}\lambda_{max}]$ and thus $k_{max} = \frac{2\pi}{\lambda_{min}}$. Since $(u, v, w) = -\omega_i - \omega_r$ and both are unit direction vectors, each component can have a value in range [-2, 2].
- for simplification, assume$[\lambda_{min,}\lambda_{max}] = [400nm, 700nm]$.

We get:

$$\begin{aligned} x_{max} &= \|i\| * k_{max} * w_{max} * h_{max} \\ &= k_{max} * w_{max} * h_{max} \\ &= 2 * (\frac{2\pi}{4 * 10^{-7}m}) * 1.5 * 10^{-7} \\ &= 1.5\pi \end{aligned} \tag{1.26}$$

and it follows for our interval $I = [0, 1.5\pi]$.

Next we are going to find the value for M. Since the exponential function is monotonically growing (on the interval I) and the derivative of the **exp** function is the exponential function itself, we can find such an M:

$$\begin{aligned} M &= e^{x_{max}} \\ &= exp(1.5\pi) \end{aligned}$$

and $|f^{(n+1)}(x)| \leq M$ holds. With

$$\begin{aligned} |E_n(x_{max})| &\leq \frac{M}{(n+1)!}|x_{max} - a|^{n+1} \\ &= \frac{exp(1.5\pi) * (1.5\pi)^{n+1}}{(n+1)!} \end{aligned} \tag{1.27}$$

we now can find a value of n for a given bound, i.e. we can find an value of $N \in \mathbb{N}$ s.t. $\frac{exp(1.5\pi)*(1.5\pi)^{N+1}}{(N+1)!} \leq \epsilon$. With Octave/Matlab we can see:

- if N=20 then $\epsilon \approx 2.9950 * 10^{-4}$
- if N=25 then $\epsilon \approx 8.8150 * 10^{-8}$
- if N=30 then $\epsilon \approx 1.0050 * 10^{-11}$

With this approach we have that $\sum_{n=0}^{25} \frac{(ikwh)^n}{n!} \mathcal{F}\{h^n\}(\alpha, \beta)$ is an approximation of $P(u,v)$ with error $\epsilon \approx 8.8150 * 10^{-8}$. This means we can precompute 25 Fourier Transformations in order to approximate P(u,v) having an error $\epsilon \approx 8.8150 * 10^{-8}$.

Using now our approximation for $P_{dtft} = \mathcal{F}^{-1}\{p\}(u,v)$ for the tristimulus value X, we will get:

$$\begin{aligned} X &= C(w_i, w_r) \int_\lambda \langle \left| P_{dtft}(\frac{2\pi u}{\lambda}, \frac{2\pi v}{\lambda}) \right|^2 \rangle S_x(\lambda) d\lambda \\ &= C(w_i, w_r) \int_\lambda \left| \sum_{n=0}^{N} \frac{(wk)^n}{n!} \mathcal{F}^{-1}\{i^n h^n\}(\frac{2\pi u}{\lambda}, \frac{2\pi v}{\lambda}) \right|^2 S_x(\lambda) d\lambda \end{aligned} \tag{1.28}$$

1.8.4 Sampling: Gaussian Window

Practically, we cannot compute the DTFT $A.3$ numerically due to finite computer arithmetic, since w is a continuous function for the DTFT. The DFT $A.4$ of a discrete height field patch is equivalent to the DTFT of an infinitely periodic function consisting of replicas of the same discrete patch. By windowing with a window function that is zero outside the central replica, the convolution of either the DFT or the DTFT of height field with the Fourier Transform of the window becomes equivalent.

Let $window_g$ denote the gaussian window with $4\sigma_s$ μm where $\sigma_f = \frac{1}{2\pi\sigma_s}$ let us further substitute $\mathbf{t}(\mathbf{x}, \mathbf{y}) = i^n h(x,y)^n$

$$\mathcal{F}^{-1}_{dtft}\{\mathbf{t}\}(u,v) = \mathcal{F}^{-1}_{fft}\{\mathbf{t}\}(u,v) window_g(\sigma_f) \tag{1.29}$$

Therefore we can deduce the following expression from this:

$$\begin{aligned}
\mathcal{F}^{-1}_{dtft}\{\mathbf{t}\}(u,v) &= \int_{-\infty}^{\infty}\int_{-\infty}^{\infty} F^{-1}_{fft}\{\mathbf{t}\}(w_u,w_v)\phi(u-w_u,v-w_v)dw_u dw_v \\
&= \int_{-\infty}^{\infty}\int_{-\infty}^{\infty}\sum_i\sum_j F^{-1}_{fft}\{\mathbf{t}\}(w_u,w_v) \\
&\quad \delta(w_u-w_i,w_v-w_j)\phi(u-w_u,v-w_v)dw_u dw_v \\
&= \sum_i\sum_j\int_{-\infty}^{\infty}\int_{-\infty}^{\infty} F^{-1}_{fft}\{\mathbf{t}\}(w_u,w_v) \\
&\quad \delta(w_u-w_i,w_v-w_j)\phi(u-w_u,v-w_v)dw_u dw_v \\
&= \sum_i\sum_j F^{-1}_{fft}\{\mathbf{t}\}(w_u,w_v)\phi(u-w_u,v-w_v) \qquad (1.30)
\end{aligned}$$

where

$$\phi(x,y) = \pi e^{-\frac{x^2+y^2}{2\sigma_f^2}} \qquad (1.31)$$

1.8.5 Final Expression

As the last step of our series of derivations, we plug all our findings together to one big equation in order to compute the color for each pixel on our mesh in the CIE_{XYZ} colorspace. For any given heigh-field $h(x,y)$ representing a small patch of a nano structure of a surface and the direction vectors w_s and w_r from figure **??** the resulting color caused by the effect of diffraction can be computed like: Let

$$P_\lambda(u,v) = F^{-1}_{fft}\{i^n h^n\}(\frac{2\pi u}{\lambda},\frac{2\pi v}{\lambda}) \qquad (1.32)$$

Then our final expression using our previous derivations will look like:

$$\begin{aligned}
\begin{pmatrix}X\\Y\\Z\end{pmatrix} = C(\omega_i,\omega_r)\int_\lambda \sum_{n=0}^{N}\frac{(wk)^n}{n!}\sum_{(r,s)\in\mathcal{N}_1(u,v)}|P_\lambda(u-w_r,v-w_s)|^2 \\
\phi(u-w_r,v-w_s)\begin{pmatrix}S_x(\lambda)\\S_y(\lambda)\\S_z(\lambda)\end{pmatrix}d\lambda
\end{aligned} \qquad (1.33)$$

where $\phi(x,y) = \pi e^{-\frac{x^2+y^2}{2\sigma_f^2}}$ is the Gaussian window 1.8.4.

1.9 Alternative Approach

1.9.1 PQ factors

In this section we are presenting an alternative approach to the previous Gaussian window approach 1.8.4 in order to solve the issue working with $DTFT$ instead the DFT. We assume, that a given surface S is covered by a number of replicas

of a provided representative surface patch f. In a simplified, one dimensional scenario, mathematically speaking, f is assumed to be a periodic function, i.e. $\forall x \in \mathbb{R} : f(x) = f(x + nT)$, where T is its period and $n \in \mathbb{N}_0$. Thus, the surfaces can be written formally as:

$$S(x) = \sum_{n=0}^{N} f(x + nT) \tag{1.34}$$

What we are looking for is an identity for the inverse Fourier transform of our surface S, required in order to simplify the (X, Y, Z) colors from 1.28:

$$\begin{aligned} \mathcal{F}^{-1}\{S\}(w) &= \int f(x)e^{iwx}dx \\ &= \int_{-\infty}^{\infty} \sum_{n=0}^{N} f(x + nT)e^{iwx}dx \\ &= \sum_{n=0}^{N} \int_{-\infty}^{\infty} f(x + nT)e^{iwx}dx \end{aligned} \tag{1.35}$$

Next, apply the following substitution $x + nT = y$ which will lead us to:

$$\begin{aligned} x &= y - nT \\ dx &= dy \end{aligned} \tag{1.36}$$

Plugging this substitution back into equation 1.35 we will get:

$$\begin{aligned} \mathcal{F}^{-1}\{S\}(w) &= \sum_{n=0}^{N} \int_{-\infty}^{\infty} f(x + nT)e^{iwx}dx \\ &= \sum_{n=0}^{N} \int_{-\infty}^{\infty} f(y)e^{iw(y-nT)}dy \\ &= \sum_{n=0}^{N} e^{-iwnT} \int_{-\infty}^{\infty} f(y)e^{iwy}dy \\ &= \sum_{n=0}^{N} e^{-iwnT} \mathcal{F}^{-1}\{f\}(w) \\ &= \mathcal{F}^{-1}\{f\}(w) \sum_{n=0}^{N} e^{-iwnT} \end{aligned} \tag{1.37}$$

We used the fact that the exponential term e^{-iwnT} is a constant factor when integrating along dy and the identity for the inverse Fourier transform of the function f. Next, let us examine the series $\sum_{n=0}^{N} e^{-iwnT}$ closer:

$$\begin{aligned} \sum_{n=0}^{N} e^{-uwnT} &= \sum_{n=0}^{N} (e^{-uwT})^n \\ &= \frac{1 - e^{iwT(N+1)}}{1 - e^{-iwT}} \end{aligned} \tag{1.38}$$

We recognize the geometric series identity for the left-hand-side of equation 1.38. Since our series is bounded, we can simplify the right-hand-side of equation 1.38.

Note that e^{-ix} is a complex number. Every complex number can be written in its polar form, i.e.

$$e^{-ix} = cos(x) + isin(x) \tag{1.39}$$

Using the following trigonometric identities

$$\begin{aligned} cos(-x) &= cos(x) \\ sin(-x) &= -sin(x) \end{aligned} \tag{1.40}$$

combined with 1.39 we can simplify the series 1.38 even further to:

$$\frac{1 - e^{iwT(N+1)}}{1 - e^{-iwT}} = \frac{1 - cos(wT(N+1)) + isin(wT(N+1))}{1 - cos(wT) + isin(wT)} \tag{1.41}$$

Equation 1.41 is still a complex number, denoted as $(p + iq)$. Generally, every complex number can be written as a fraction of two complex numbers. This implies that the complex number $(p + iq)$ can be written as $(p + iq) = \frac{(a+ib)}{(c+id)}$ for any $(a + ib), (c + id) \neq 0$. Let us use the following substitutions:

$$\begin{aligned} a &:= 1 - cos(wT(N+1)) & b &= sin(wT(N+1)) \\ c &= 1 - cos(wT) & d &= sin(wT) \end{aligned} \tag{1.42}$$

Hence, using 1.42, it follows

$$\frac{1 - e^{iwT(N+1)}}{1 - e^{-iwT}} = \frac{(a + ib)}{(c + id)} \tag{1.43}$$

By rearranging the terms, it follows $(a + ib) = (c + id)(p + iq)$ and by multiplying its right hand-side out we get the following system of equations:

$$\begin{aligned} (cp - dq) &= a \\ (dp + cq) &= b \end{aligned} \tag{1.44}$$

After multiplying the first equation of 1.44 by c and the second by d and then adding them together, we get using the law of distributivity new identities for p and q:

$$\begin{aligned} p &= \frac{(ac + bd)}{c^2 + d^2} \\ q &= \frac{(bc + ad)}{c^2 + d^2} \end{aligned} \tag{1.45}$$

Using some trigonometric identities and putting our substitution from 1.42 for a, b, c, d back into the current representation 1.45 of p and q we will get:

$$p = \frac{1}{2} + \frac{1}{2}\left(\frac{cos(wTN) - cos(wT(N+1))}{1 - cos(wT)}\right)$$
$$q = \frac{sin(wT(N+1)) - sin(wTN) - sin(wT)}{2(1 - cos(wT))} \tag{1.46}$$

Since we have seen, that $\sum_{n=0}^{N} e^{-uwnT}$ is a complex number and can be written as $(p + iq)$, we now know an explicit expression for p and q. Therefore, the one dimensional inverse Fourier transform of S is equal:

$$\begin{aligned}\mathcal{F}^{-1}\{S\}(w) &= \mathcal{F}^{-1}\{f\}(w) \sum_{n=0}^{N} e^{-iwnT} \\ &= (p + iq)\mathcal{F}^{-1}\{f\}(w)\end{aligned} \tag{1.47}$$

Now lets consider our actual problem description. Given a patch of a nano-scaled sureface snake shed represented as a two dimensional heightfield $h(x, y)$. We once again assume that this provided patch is representing the whole surface S of our geometry by some number of replicas of itself. Therefore, $S(x, y) = \sum_{n=0}^{N} h(x + nT_1, y + mT_2)$, assuming the given height field has the dimensions T_1 by T_2. In order to derive an identity for the two dimensional inverse Fourier transformation of S we can similarly proceed like we did to derive equation 1.47.

$$\begin{aligned}\mathcal{F}^{-1}\{S\}(w_1, w_2) &= \int_{-\infty}^{\infty}\int_{-\infty}^{\infty} \sum_{n_2=0}^{N_1}\sum_{n_2=0}^{N_2} h(x_1 + n_1T_1, x_2 + n_2T_2)e^{iw(x_1+x_2)}dx_1dx_2 \\ &= \int_{-\infty}^{\infty}\int_{-\infty}^{\infty} \sum_{n_2=0}^{N_1}\sum_{n_2=0}^{N_2} h(y_1, y_2)e^{iw((y_1-n_1T_1)+(y_2+n_2T_2))}dx_1dx_2 \\ &= \sum_{n_2=0}^{N_1}\sum_{n_2=0}^{N_2} \int_{-\infty}^{\infty}\int_{-\infty}^{\infty} h(y_1, y_2)e^{iw(y_1+y_2)}e^{-iw(n_1T_1+n_2T_2)}dy_1dy_2 \\ &= \sum_{n_2=0}^{N_1}\sum_{n_2=0}^{N_2} e^{-iw(n_1T_1+n_2T_2)} \int_{-\infty}^{\infty}\int_{-\infty}^{\infty} Box(y_1, y_2)e^{iw(y_1+y_2)}dy_1dy_2 \\ &= \left(\sum_{n_2=0}^{N_1}\sum_{n_2=0}^{N_2} e^{-iw(n_1T_1+n_2T_2)}\right)\mathcal{F}^{-1}\{h\}(w_1, w_2) \\ &= \left(\sum_{n_2=0}^{N_1} e^{-iwn_1T_1}\right)\left(\sum_{n_2=0}^{N_2} e^{-iwn_2T_2}\right)\mathcal{F}^{-1}\{h\}(w_1, w_2) \\ &= (p_1 + iq_1)(p_2 + iq_2)\mathcal{F}^{-1}\{h\}(w_1, w_2) \\ &= ((p_1p_2 - q_1q_2) + i(p_1p_2 + q_1q_2))\mathcal{F}^{-1}\{h\}(w_1, w_2) \\ &= (p + iq)\mathcal{F}^{-1}_{DTFT}\{h\}(w_1, w_2)\end{aligned} \tag{1.48}$$

Where we have defined

$$\begin{aligned}p &:= (p_1p_2 - q_1q_2) \\ q &:= (p_1p_2 + q_1q_2)\end{aligned} \tag{1.49}$$

For the identity of equation 1.48 we made use of Green's integration rule which allowed us to split the double integral to the product of two single integrations. Also, we used the definition of the 2-dimensional inverse Fourier transform of the height field function. We applied a similar substitution like we did in 1.36, but this time twice, once for x_1 and once for x_2 separately. The last step in equation 1.48, substituting with p and q in equation 1.49 will be useful later in the implementation. The insight should be, that the product of two complex numbers is again a complex number. We will have to compute the absolute value of $\mathcal{F}^{-1}\{S\}(w_1, w_2)$ which will then be equal $(p^2+q^2)^{\frac{1}{2}} \left|\mathcal{F}^{-1}\{h\}(w_1, w_2)\right|$

1.9.2 Interpolation

In 1.9.1 we have derived an alternative approach when we are working with a periodic signal instead using the gaussian window approach from sec *sec* : *gaussianwindow*. Its main finding 1.48 that we can just integrate over one of its period instead iterating over the whole domain. Nevertheless, this main finding is using the inverse DTFT. Since we are using

We are interested in recovering an original analog signal $x(t)$ from its samples $x[t] =$

Therfore, for a given sequence of real numbers $x[n]$, representing a digital signal, its correspond continuous function is:

$$x(t) = \sum_{n=-\infty}^{\infty} x[n] sinc\left(\frac{t-nT}{T}\right) \tag{1.50}$$

which has the Fourier transformation $X(f)$ whose non-zero values are confined to the region $|f| \leq \frac{1}{2T} = B$. When $x[n]$ represents time samples at interval T of a continuous function, then the quantity $f_s = \frac{1}{T}$ is known as its sample rate and $\frac{f_s}{2}$ denotes the Nyquist frequency. The sampling Theorem states that when a function has a Bandlimit B less than the Nyquist frequency, then $x(t)$ is a perfect reconstruction of the original function.

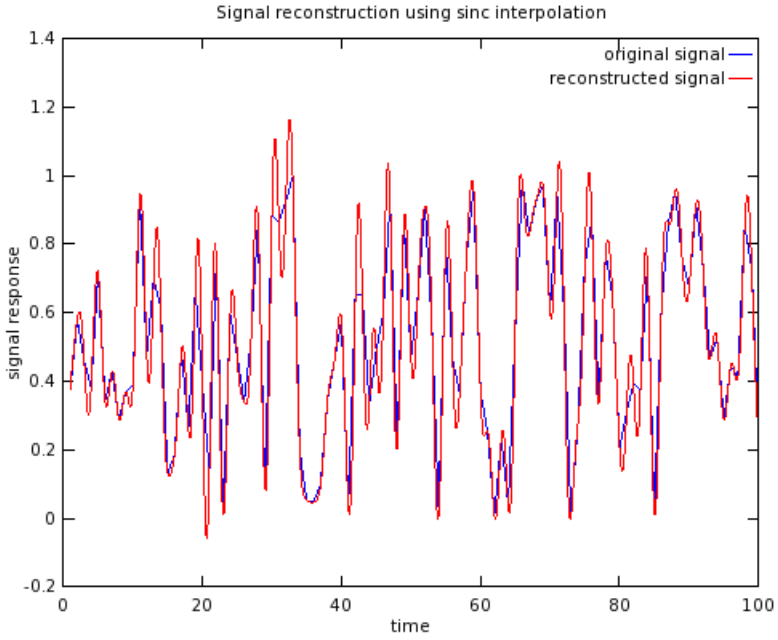

Abbildung 1.3: Comparission between a given random one dimensional input signal $s(t)$ and its sinc interpolation $\hat{s}(t)$. Notice that for the interpolation there were $N = 100$ samples from the original signal provided.

Kapitel 2

Evaluation and data acquisition

2.1 Data Acquisition

Our goal is to perform physically accurate simulations of diffraction effects on natural gratings. As for every simulation, its outcome highly depends on the provided input data we also require measurements[1] of real natural gratings. For that purpose, samples of skins of Xenopeltis and Elaphe snake species were fixed on a glass plate and then, by using an Atomic Force Microscope (AFM), their surface topography was measured and stored as grayscale images, indicating the depth. In general, an ADM is is a microscope that uses a tiny probe mounted on a cantilever to scan the surface of an object. The probe is extremely close to the surface, but does not touch it. As the probe traverses the surface, attractive and repulsive forces arising between it and the atoms on the surface induce forces on the probe that bend the cantilever. The amount of bending is measured and recorded, providing a map of the atoms on the surface. Atomic force microscopes is a very high-resolution type of scanning probe microscopy, with demonstrated resolution on the order of fractions of a nanometer, more than 1000 times better than the optical diffraction limit.

2.2 Diffraction Gratings

In order to evaluate the quality of our simulations, it is important to understand what a diffraction grating actually is. An idealised diffraction grating like in figure 2.2 is made of a large number of parallel, evenly spaced slits in an opaque medium. In general, if the spacing between slits is wider than the wavelength of the incoming light, then the better we can observe how the light is diffracted on the grating. Simply speaking, each slit in the grating acts as a point light source from which light spreads and propagates in all directions. According to Huygen's Principle the outgoing light may have a different outgoing angle as it hat initially. Figure 2.1 illustrates this behaviour for a monochromatic light

[1] All measured data has been provided by the Laboratory of Artificial and Natural Evolition at Genava - Website:`www.lanevol.org`

source passing through a grating and shows that the the outgoing angle will be different from the incident angle. Hence, the diffracted light **??** is composed of the sum of interfering wave components emanating from each slit in the grating.

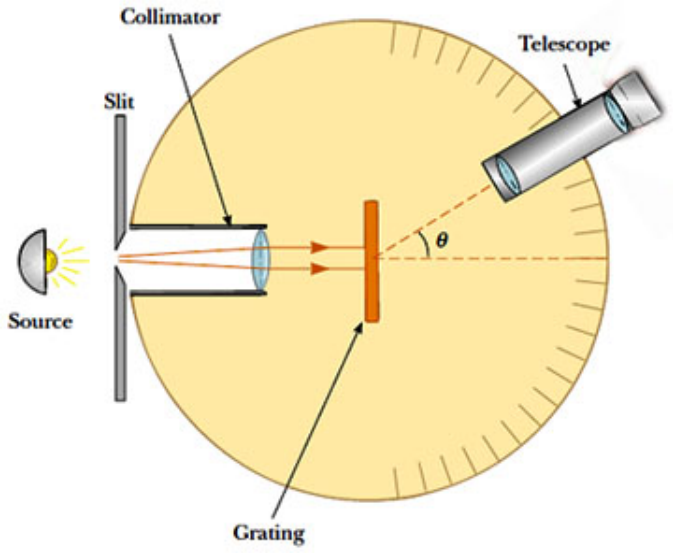

Abbildung 2.1: Spectometer: When a beam of monochromatic light passes through a grating placed in a spectrometer, images of the sources can be seen through the telescope at different angles.

Suppose that a monochromatic light source is directed at the grating, parallel to its axis as shown in figure 2.1. Let the distance between successive slits be equal the value d.

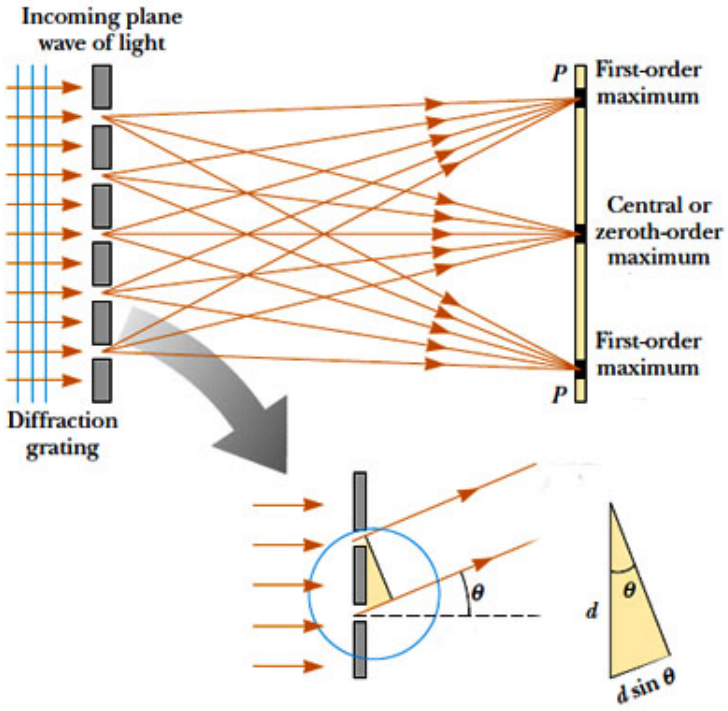

Abbildung 2.2: Light directed to parallel to grating:

The observable diffraction pattern is the result of interference effects among outgoing wavelets according to Huygen's Principle. The path difference between waves from any two adjacent slits can be derived by drawing a perpendicular line between the parallel waves. Applying some trigonometry, this path difference is $dsin(\theta)$. If the path difference equals one wavelength or a multiple of the wave's wavelength, the emerging, reflected waves from all slits will be in phase and a bright line will be observed at that point. Therefore, the condition for maxima in the interference pattern at the angle θ is:

$$dsin(\theta) = m\lambda \tag{2.1}$$

where $m \in \mathbb{N}_0$ is the order of diffraction. Because d is very small for a diffraction grating, a beam of monochromatic light passing through a diffraction grating is split into very narrow bright fringes at large angles θ.

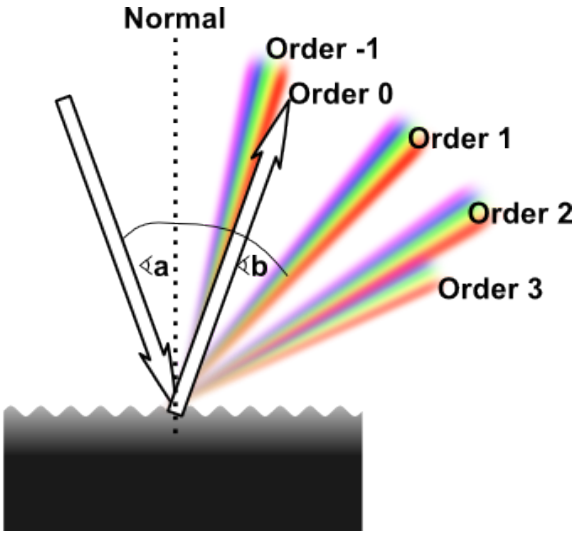

Abbildung 2.3: Different Orders of diffraction

When a narrow beam of white light is directed at a diffraction grating along its axis, instead of a monochromatic bright fringe, a set of colored spectra are observed on both sides of the central white band as shown in figure 2.3.

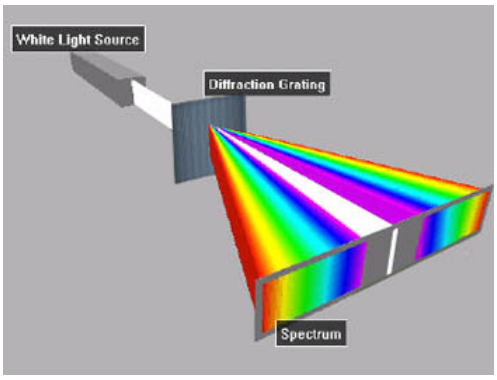

Abbildung 2.4: White Light beam causes coloured diffraction spectra

Since the angle θ increases with wavelength λ, red light, which has the longest wavelength, is diffracted through the largest angle. Similarly violet light has the shortest wavelength and is therefore diffracted the least. This relationship between angle and wavelength is illustrated in figure 2.4. Thus, white light is split into its component colors from violet to red light. The spectrum is repeated in the different orders of diffraction, emphasizing certain colors differently, depending on their order of diffraction like shown in figure 2.3. Note that only the zero order spectrum is pure white. Figure 2.5 shows the relative intensity resulting when a beam of light hits a diffraction grating for different number of periods. From the graph we recognise that the more slits a grating has, the sharper more slopes the function of intensity gets. This is similar like saying that, the more periods a grating has, the sharper the diffracted color spectrum

gets like shown in figure 2.6.

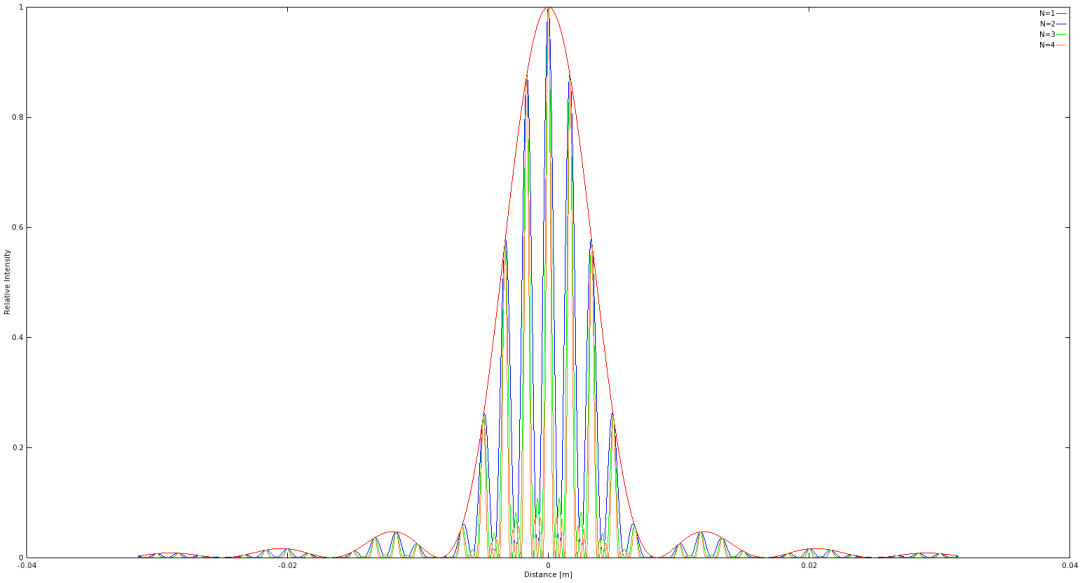

Abbildung 2.5: Relative intensities of a diffracted beam of light at wavelength $\lambda = 500nm$ on a grating for different number of periods N width slit width of 30 microns and slit separation of 0.15 mm each. The viewer is 0.5m apart from the grating.

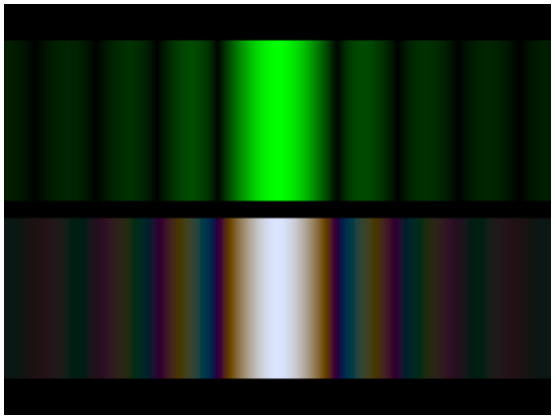

(a) one slit

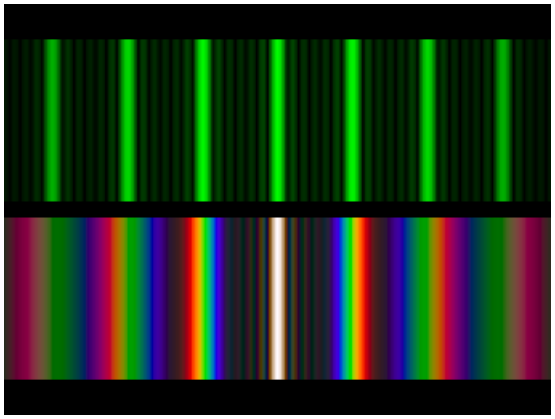

(b) seven slits

Abbildung 2.6: Difference of diffraction pattern between a monochromatic (top) and a white (bottom) light spectra for different number of slits.

2.3 Evaluation

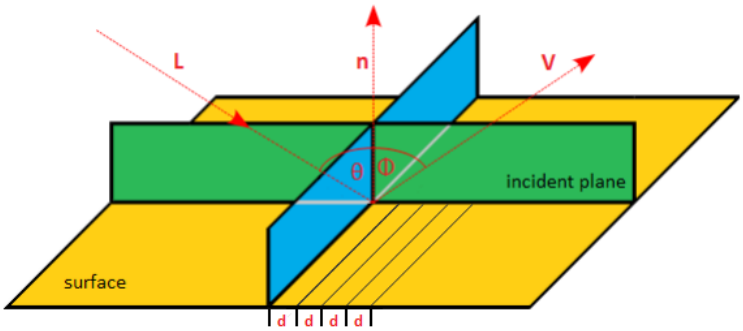

Abbildung 2.7: Experimental setup for evaluation: A light beam with direction L hits the surface, representing a grating pattern with periodicity d, at the incident plane relative to the surface normal n at angle θ and emerges at angle ϕ with direction V.

The physical reliability of our BRDF models has been verified by applying those on various patches which are a synthetic blazed grating, an Elaphe and a Xenopeltis snake shed sample patch. We compared the resulting response against the response resulting by the grating equation, which models the relationship between the grating spacing and the angles of the incident and diffracted beams of light. Figure 2.7 illustrates the geometrical setup for our evaluation approach: A monochromatic beam of light with wavelength λ hits a surface with periodicity d at an angle θ relative to the normal n along its incident plane. The beam emerges from the surface at the angle ϕ.

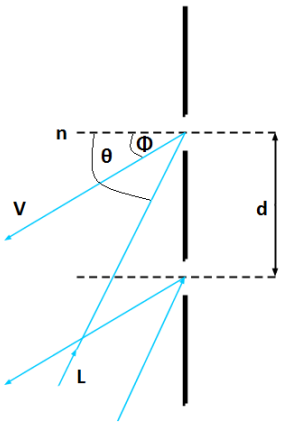

Abbildung 2.8: Reflecting grating: When the incident light direction is not parallel to its axis at the grating, there is another $sin(\phi)$ involved. See also the grating equation 2.2.

The maximum in intensity is given by the grating equation derived from the

equation 2.1 following figure 2.8:

$$sin(\theta) = sin(\phi) + \frac{m\lambda}{d} \tag{2.2}$$

In our evaluation we are interested in the first order diffraction, i.e. m equals one which. We further assume that the incident light direction ω_i is given. In contrast the direction of the reflected wave ω_r is not given. In Mathematics, a three dimensional direction vector is fully defined by two two angles, i.e. it can be represented by spherical coordinates with radius $r = 1$. By convention, we denote those two vectors by θ and ϕ like in figure 2.7. Hence, θ_i, ϕ_i and ϕ_r are given constants whereas θ_i is a free parameter for our evaluation simulation. Therefore, we are going to compare the maxima for peak viewing angles corresponding to each wavelength using data produced by our method against the maxima resulting by the grating equation 2.2.

2.3.1 Precomputation

For evaluation purposes we have implemented our BRDF models in java. We once again use our geometrical setup as illustrated in figure **??** where θ_i, ϕ_i and ϕ_r are provided as input values and θ_i is a free parameter. Within our evaluation we have set them to $\theta_i = 75$ $\phi_i = 0$ $\phi_r = 180$ degrees. The wavelength space Λ and the range Θ of our free parameter θ_i are discretized in equidistant steps whereas their step sizes are given as input arguments for our Java program:

$$\Lambda = \{\lambda | \lambda = \lambda_{min} + k \cdot \lambda_{step}, \quad k \in \{0, .., C-1\}\} \tag{2.3}$$

where $\lambda_{step} = \frac{\lambda_{max} - \lambda_{min}}{C-1}$ and C is the discretisation level of the lambda space. We similarly discretise the angle space by predefining an minimal and maximal angle boundary and $ceil(angMax - angMin)/angInc$ is the number of angles. Our Java BRDF model implementations are applied on the grid $[\Lambda, \Theta]$ and will store their spectral response in a matrix

$$R = \{response(\lambda_i, \theta_r^j) | i \in Index(\Lambda), \quad j \in Index(\Theta)\} \tag{2.4}$$

We will plot this matrix and compare its graph against the grating equation for similar condition like in stated in algorithm 2.1.

Algorithm 2.1 Vertex diffraction shader

load matrix R 2.4
$\lambda_{count} = |\Lambda|$
$\lambda_{inc} = \frac{\lambda_{max} - \lambda_{min}}{\lambda_{count}}$
$\lambda = \lambda_{min} + \lambda_{inc} \cdot (-1 + [1 : \lambda_{count}])$
$[maxCmaxI] = max(R)$
$viewAngForMax = angMin + angInc \cdot (maxI - 1)$
$thetaV = asin\left(\frac{\lambda}{d} - \sin\left(\frac{\theta_I \pi}{180}\right)\right) \cdot \frac{180}{\pi}$
$plot(\lambda, viewAngForMax)$ ▷ graph resulting by our brdf model
$plot(lambda, thetaV)$ ▷ graph resulting by grating equation

2.3.2 Evaluation graphs

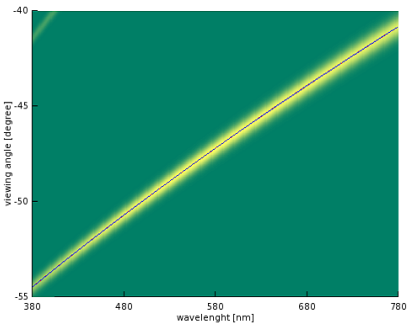

(a) Blaze grating

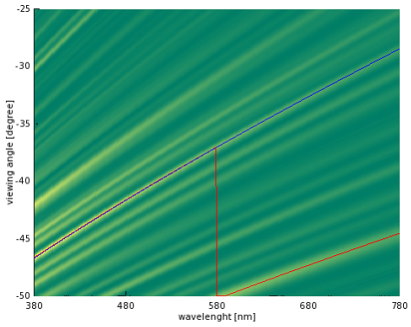

(b) Xenopeltis grating

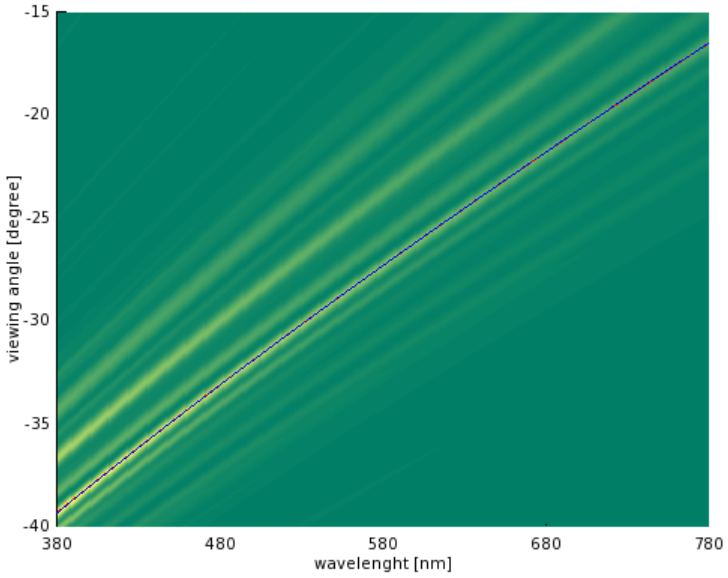

(c) Elaphe grating

Abbildung 2.9: Reflectance obtained by using the shading approach described in algorithm **??** simulating a BRDF which models the effect of diffraction at different viewing angles over the spectrum of visible light.

In this section we discuss the quality of our BRDF models applied to different surface structures. For that purpose we compare the resulting relative reflectance computed as described in section 2.3.1 for each of our BRDF models to the idealized grating equation 2.2.

Patch	Mean[mm]	Variance[mm]
Blazed grating **??**	2500.34	0.16
Elaphe grating **??**	1144.28	0.15
Xenopeltis grating **??**	1552.27	0.45

Tabelle 2.1: Statistics of periodicity d of our used gratings **??** estimated by using the grating equation 2.2. This table was provided by Mr. D.Singh.

Figure 2.9 shows the reflectance graphs resulting by the shading approach of sampling the whole lambda space descriped in algorithm **??**. This evaluation has been applied to different idealized periodic structures, namely to the Blaze- 2.9(a), Elaphe- 2.9(c) and Xenopeltis grating 2.9(b), using an illumination angle $\theta_i = 75$ degrees. Note that higher response values are plotted in yellow and lower values in green. For each of the graphs we determine the viewing angles with peak reflectance for various wavelengths and then plot this peak viewing angles against their wavelength as solid red curves. The blue curve represents diffraction angles for an idealized periodic structure with a certain periodicity d according to the grating equation 2.2. The corresponding periodicity for every grating structure is estimated using the precomputed response data using again the grating equation and are tabulated in table 2.1.

The red and blue curve are closely overlapping in our figures 2.9(a) and 2.9(c). For Blaze and Elaphe there is only diffraction along only along one direction perceivable. Since the Blazed grating is synthetic we use its exact periodicity to plot the blue curve instead of estimating it. The Xenopeltis grating is evaluated just along the direction for the finger like structures. For Xenopeltis it is interesting to see that the red curve for the peak viewing angle toggles between two ridges corresponding to two different periodicities. this happens because there are multiple sub regions of the nanostructure with slightly different orientations and periodicity. Each sub region carves out a different yellowish ridge. depending on the viewing angle, reflectance due to one such subregion can be higher than from the others.

Figure 2.10 shows the evaluation plots for the (N_{min}, N_{max}) shading approach which integrates over a reduced wavelength spectrum applied to the Blaze- 2.10(b) and the Elaphe-grating 2.10(b). This optimization approach is mentioned within the discussion section of the implementation chapter **??** as a run-time complexity enhancement of the whole lambda space sampling approach 2.9. The response curve again closely matches the corresponding grating equation curve for both evaluation graphs and also look similar to the corresponding evaluation plots when integrating over the whole lambda space shown previously in figure . Therefore we may assume this optimization to be valid.

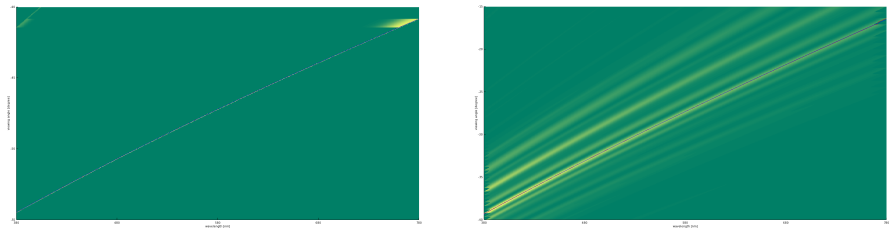

(a) Blaze grating (b) Elaphe grating

Abbildung 2.10: Reflectance obtained using $N_{min}N_{max}$ optimization apporach

Last let us consider the evaluation graphs of the PQ approach **??** in figure 2.11. The PQ approach assumes the given grating being periodically distributed on a shape's surface. For this approach we have plotted evaluation graphs of the Blaze- 2.11(a) and Elaphe grating 2.11(b). For both graphs their response curves have some similarities but also some differences compared to their corresponding grating equation curve. We could say that the response curve of the blaze grating is weakly oscillating around the grating equation curve (blue) but basically following it even there are some outliers. The response curve of the Elpahe grating is not following its corresponding first order grating equation curve rather another response curve for the PQ approach. This could be due to the assumption of the PQ approach that a given patch must be periodically distributed along the surface which is actually not that case. Nevertheless, the red curve fits one of the response curves.

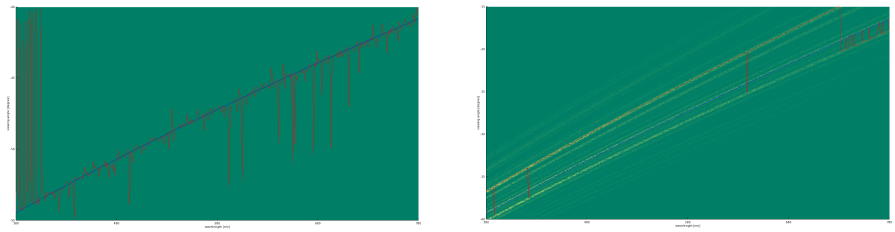

(a) Blaze grating (b) Elaphe grating

Abbildung 2.11: Reflectance obtained using PQ optimization apporach

Anhang A

Signal Processing Basics

A signal is a function that conveys information about the behavior or attributes of some phenomenon. In the physical world, any quantity exhibiting variation in time or variation in space (such as an image) is potentially a signal that might provide information on the status of a physical system, or convey a message between observers.

The Fourier Transform is an important image processing tool which is used to decompose an image into its sine and cosine components. The output of the transformation represents the image in the Fourier or frequency domain, while the input image is the spatial domain equivalent. In the Fourier domain image, each point represents a particular frequency contained in the spatial domain image.

A.1 Fourier Transformation

The Fourier-Transform is a mathematical tool which allows to transform a given function or rather a given signal from defined over a time- (or spatial-) domain into its corresponding frequency-domain.

Let f an measurable function over $\mathbb{R}^n$. Then, the continuous Fourier Transformation(**FT**), denoted as $\mathcal{F}\{f\}$ of f, ignoring all constant factors in the formula, is defined as:

$$\mathcal{F}_{FT}\{f\}(w) = \int_{\mathbb{R}^n} f(x)e^{-iwt}dt \tag{A.1}$$

whereas its inverse transform is defined like the following which allows us to obtain back the original signal:

$$\mathcal{F}_{FT}^{-1}\{f\}(w) = \int_{\mathbb{R}} \mathcal{F}\{w\}e^{iwt}dt \tag{A.2}$$

Usual w is identified by the angular frequency which is equal $w = \frac{2\pi}{T} = 2\pi v_f$. In this connection, T is the period of the resulting spectrum and v_f is its corresponding frequency.

By using Fourier Analysis, which is the approach to approximate any function by sums of simpler trigonometric functions, we gain the so called Discrete Time Fourier Transform (in short **DTFT**). The DTFT operates on a discrete

function. Usually, such an input function is often created by digitally sampling a continuous function. The DTFT itself is operation on a discretized signal on a continuous, periodic frequency domain and looks like the following:

$$\mathcal{F}_{DTFT}\{f\}(w) = \sum_{-\infty}^{\infty} f(x)e^{-iwk} \tag{A.3}$$

Note that the DTFT is not practically suitable for digital signal processing since there a signal can be measured only in a finite number of points. Thus, we can further discretize the frequency domain and will get then the Discrete Fourier Transformation (in short **DFT**) of the input signal:

$$\mathcal{F}_{DFT}\{f\}(w) = \sum_{n=0}^{N-1} f(x)e^{-iw_n k} \tag{A.4}$$

Where the angular frequency w_n is defined like the following $w_n = \frac{2\pi n}{N}$ and N is the number of samples within an equidistant period sampling.

Any continuous function $f(t)$ can be expressed as a series of sines and cosines. This representation is called the Fourier Series (denoted by FS) of $f(t)$.

$$f(t) = \frac{1}{2}a_0 + \sum_{n=1}^{\infty} a_n cos(nt) + \sum_{n=1}^{\infty} b_n cos(nt) \tag{A.5}$$

where

$$\begin{aligned} a_0 &= \int_{-\pi}^{\pi} f(t)dt \\ a_n &= \frac{1}{\pi}\int_{-\pi}^{\pi} f(t)cos(nt)dt \\ b_n &= \frac{1}{\pi}\int_{-\pi}^{\pi} f(t)sin(nt)dt \end{aligned} \tag{A.6}$$

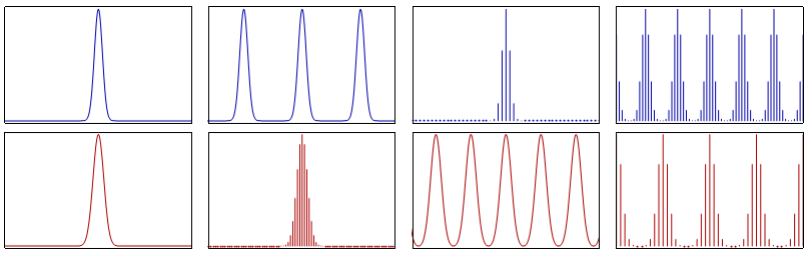

Abbildung A.1: Relationship[1] between the continuous Fourier transform and the discrete Fourier transform: Left column: A continuous function (top) and its Fourier transform $A.1$ (bottom). Center-left column: Periodic summation of the original function (top). Fourier transform (bottom) is zero except at discrete points. The inverse transform is a sum of sinusoids called Fourier series $A.5$. Center-right column: Original function is discretized (multiplied by a Dirac comb) (top). Its Fourier transform (bottom) is a periodic summation (DTFT) of the original transform. Right column: The DFT $A.4$ (bottom) computes discrete samples of the continuous DTFT $A.3$. The inverse DFT (top) is a periodic summation of the original samples.

Spetail signal $f(t)$ is	Operator	Transformed frequency signal $\hat{f}(\omega)$ is
continuous and periodic in t	FS $A.5$	only discrete in ω
only continuous in t	FT $A.1$	only continuous in ω
only discrete in t	DTFT $A.3$	continuous and periodic in ω
discrete and periodic in t	DFT $A.4$	discrete and periodic in ω

Tabelle A.1: Fourier operator to apply for a given spatial input signal and the properties of its resulting output signal in frequency space

A.2 Convolution

The convolution $f * g$ of two functions f, g: $\mathbb{R}^n \to \mathbb{C}$ is defined as:

$$(f * g)(t) = \int_{\mathbb{R}^n} f(t)g(t-x)dx \tag{A.7}$$

Note that the Fourier transform of the convolution of two functions is the product of their Fourier transforms. This is equivalent to the fact that Convolution in spatial domain is equivalent to multiplication in frequency domain. Therefore, the inverse Fourier transform of the product of two Fourier transforms is the convolution of the two inverse Fourier transforms. Last an illustration of the relationships between the previous presented Fourier transformations and different given input signals. First an concrete example shown in Figure $A.1$. Table $A.1$ tells what Fourier transformation operator has to be applied to which kind of input signal and what properties its resulting Fourier transform will have.

A.3 Taylor Series

Taylor series is a representation of a function as an infinite sum of terms that are calculated from the values of the function's derivatives at a single point.

The Taylor series $\mathcal{T}$ of a real or complex-valued function $f(x)$ that is infinitely differentiable at a real or complex number a is the power series:

$$\mathcal{T}(f;a)(x) = \sum_{n=0}^{\infty} \frac{f^n(a)}{n!}(x-a)^n \tag{A.8}$$

[1] image of illustration has been taken from wikipedia

Anhang B

Appendix

B.1 Schlick's approximation

The Fresnel's equations describe the reflection and transmission of electromagnetic waves at an interface. That is, they give the reflection and transmission coefficients for waves parallel and perpendicular to the plane of incidence. Schlick's approximation is a formula for approximating the contribution of the Fresnel term where the specular reflection coefficient R can be approximated by:

$$R(\theta) = R_0 + (1 - R_0)(1 - \cos\theta)^5 \tag{B.1}$$

and

$$R_0 = \left(\frac{n_1 - n_2}{n_1 + n_2}\right)^2$$

where θ is the angle between the viewing direction and the half-angle direction, which is halfway between the incident light direction and the viewing direction, hence $\cos\theta = (H \cdot V)$. And n_1, n_2 are the indices of refraction of the two medias at the interface and R_0 is the reflection coefficient for light incoming parallel to the normal (i.e., the value of the Fresnel term when $\theta = 0$ or minimal reflection). In computer graphics, one of the interfaces is usually air, meaning that n_1 very well can be approximated as 1.

B.2 Spherical Coordinates

$$\forall \begin{pmatrix} x \\ y \\ z \end{pmatrix} \in \mathbb{R}^3 : \exists r \in [0, \infty) \exists \phi \in [0, 2\pi] \exists \theta \in [0, \pi] \text{ s.t.}$$

$$\begin{pmatrix} x \\ y \\ z \end{pmatrix} = \begin{pmatrix} rsin(\theta)cos(\phi) \\ rsin(\theta)sin(\phi) \\ rcos(\theta) \end{pmatrix}$$

B.3 Tangent Space

The concept of tangentspace-transformation of tangent space is used in order to convert a point between world and tangent space. GLSL fragment shaders require normals and other vertex primitives declared at each pixel point, which mean that we have one normal vector at each texel and the normal vector axis will vary for every texel.

Think of it as a bumpy suface defined on a flat plane. If those normals were declared in the world space coordinate system, we would have to rotate these normals every time the model is rotated, even when just for a small amount. Since the lights, cameras and other objects are usually defined in world space coordinate system, and therefore, when they are involved in an calculation within the fragment shader, we would to have to rotate them as well for every pixel. This would involve almost countless many object to world matrix transformations meed to take place at the pixel level. Therefore, instead doing so, we transform all vertex primitives into tangent space within the vertex shader.

To make this point clear an example: Even we would rotate the cube in figure *B*.1, the tangent space axis will remain aligned with respect to the face. Which practically speaking, will save us from performing many space transformations applied pixel-wise within the fragment shader and instead allows us to perform us the tangenspace transformation of every involved vertex primitive in the vertex-shader.

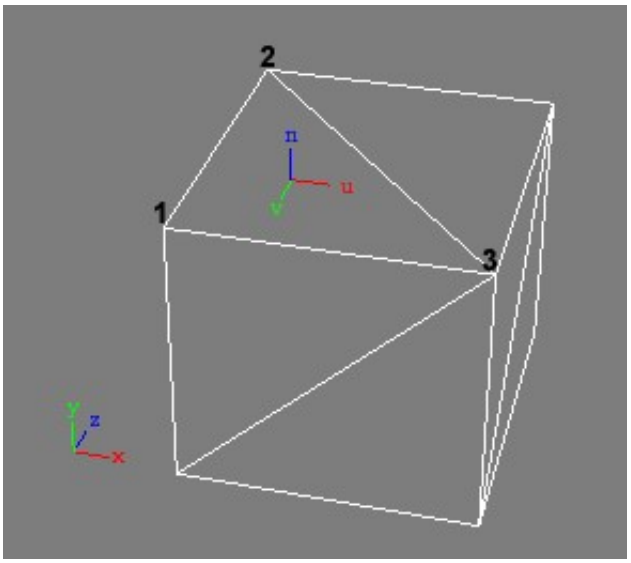

Abbildung B.1: Cube in world space (x, y, z) showing the tangen space (u, v, n) of its face $(2, 1, 3)$

Tabellenverzeichnis

Abbildungsverzeichnis

List of Algorithms

Literaturverzeichnis

[Bar07] Bartsch, Hans-Jochen: *Taschenbuch Mathematischer Formeln*. 21th edition. HASNER, 2007. – ISBN 978–3–8348–1232–2

[CT12] Cuypers T., et a.: Reflectance Model for Diffraction. In: *ACM Trans. Graph. 31, 5* (2012), September

[DSD14] D. S. Dhillon, et a.: Interactive Diffraction from Biological Nanostructures. In: *XYZ* (2014), January

[For11] Forster, Otto: *Analysis 3*. 6th edition. VIEWEG+TEUBNER, 2011. – ISBN 978–3–8348–1232–2

[I.N14] I.Newton: *Opticks, reprinted*. CreateSpace Independent Publishing Platform, 2014. – ISBN 978–1499151312

[JG04] Juan Guardado, NVIDIA: Simulating Diffraction. In: *GPU Gems* (2004). `https://developer.nvidia.com/content/gpu-gems-chapter-8-simulating-diffraction`

[MT10] Matin T.R., et a.: Correlating Nanostructures with Function: Structurral Colors on the Wings of a Malaysian Bee. (2010), August

[PAT09] Paul A. Tipler, Gene M.: *Physik für Wissenschaftler und Ingenieure*. 6th edition. Spektrum Verlag, 2009. – ISBN 978–3–8274–1945–3

[PS09] P. Shirley, S. M.: *Fundamentals of Computer Graphics*. 3rd edition. A K Peters, Ltd, 2009. – ISBN 978–1–56881–469–8

[R.H12] R.Hooke: *Micrographia, reprinted*. CreateSpace Independent Publishing Platform, 2012. – ISBN 978–1470079031

[RW11] R. Wright, et a.: *OpenGL SuperBible*. 5th edition. Addison-Wesley, 2011. – ISBN 978–0–32–171261–5

[Sta99] Stam, J.: Diffraction Shaders. In: *SIGGRPAH 99 Conference Proceedings* (1999), August

Erklärung

gemäss Art. 28 Abs. 2 RSL 05

Name/Vorname: .....

Matrikelnummer: .....

Studiengang: ……

Bachelor ☐ Master ☐ Dissertation ☐

Titel der Arbeit: .....

.....

.....

LeiterIn der Arbeit: .....

.....

Ich erkläre hiermit, dass ich diese Arbeit selbständig verfasst und keine anderen als die angegebenen Quellen benutzt habe. Alle Stellen, die wörtlich oder sinngemäss aus Quellen entnommen wurden, habe ich als solche gekennzeichnet. Mir ist bekannt, dass andernfalls der Senat gemäss Artikel 36 Absatz 1 Buchstabe o des Gesetztes vom 5. September 1996 über die Universität zum Entzug des auf Grund dieser Arbeit verliehenen Titels berechtigt ist.

.....
Ort/Datum

.....
Unterschrift